

Communication

Matrigel Tunes H9 Stem Cell-Derived Human Cerebral Organoid Development

R. Chris Estridge ¹, Jennifer E. O'Neill ² and Albert J. Keung ^{1,*}

¹ Department of Chemical & Biomolecular Engineering, North Carolina State University, Raleigh, NC 27606, USA

² Genetics Program, Department of Biological Sciences, North Carolina State University, Raleigh, NC 27606, USA; jeoneill@alumni.ncsu.edu

* Correspondence: ajkeung@ncsu.edu

Abstract: Human cerebral organoids are readily generated from human embryonic stem cells and human induced pluripotent stem cells and are useful in studying human neurodevelopment. Recent work with human cerebral organoids have explored the creation of different brain regions and the impacts of soluble and mechanical cues. Matrigel is a gelatinous, heterogenous mixture of extracellular matrix proteins, morphogens, and growth factors secreted by Engelbreth-Holm-Swarm mouse sarcoma cells. It is a core component of almost all cerebral organoid protocols, generally supporting neuroepithelial budding and tissue polarization; yet, its roles and effects beyond its general requirement in organoid protocols are not well understood, and its mode of delivery is variable, including the embedding of organoids within it or its delivery in soluble form. Given its widespread usage, we asked how H9 stem cell-derived hCO development and composition are affected by Matrigel dosage and delivery method. We found Matrigel exposure influences organoid size, morphology, and cell type composition. We also showed that greater amounts of Matrigel promote an increase in the number of choroid plexus (ChP) cells, and this increase is regulated by the BMP4 pathway. These results illuminate the effects of Matrigel on human cerebral organoid development and the importance of delivery mode and amount on organoid phenotype and composition.

Keywords: cerebral organoids; Matrigel; extracellular matrix; development; neurodevelopment; bioengineering; human; choroid plexus; differentiation



Citation: Estridge, R.C.; O'Neill, J.E.; Keung, A.J. Matrigel Tunes H9 Stem Cell-Derived Human Cerebral Organoid Development. *Organoids* **2023**, *2*, 165–176. <https://doi.org/10.3390/organoids2040013>

Academic Editor: Ernst Wolvetang

Received: 23 July 2023

Revised: 19 August 2023

Accepted: 22 September 2023

Published: 5 October 2023



Copyright: © 2023 by the authors. Licensee MDPI, Basel, Switzerland. This article is an open access article distributed under the terms and conditions of the Creative Commons Attribution (CC BY) license (<https://creativecommons.org/licenses/by/4.0/>).

1. Introduction

Human cerebral organoids are readily generated from human embryonic stem cells and human induced pluripotent stem cells and are useful in studying human neurodevelopment. As with any experimental model, there are several goals: to improve their reproducibility, complexity, and fidelity to in vivo tissues; to understand how components and protocol parameters control model phenotypes; and to expand the range of phenotypes that can be captured by the model. Recent work with human cerebral organoids has explored the creation of different brain regions [1–7] and the impacts of soluble [8,9] and mechanical cues [10,11].

Matrigel is a gelatinous, heterogenous mixture of extracellular matrix proteins, morphogens, and growth factors secreted by Engelbreth-Holm-Swarm mouse sarcoma cells [12]. Previous work has examined and quantified Matrigel components [13,14], but due to the complexity of Matrigel, it has been difficult to create a synthetic replacement. It is a core component of almost all cerebral organoid protocols, generally supporting neuroepithelial budding and tissue polarization [11,15,16]; yet, its roles and effects beyond its general requirement in organoid protocols are not well understood [14,17,18], and its mode of delivery is variable, including the embedding of organoids within it or its delivery in

soluble form [1,11,19–22]. To our knowledge, the effects of Matrigel dosage and mode of delivery on human cerebral organoids (hCOs) have not been reported.

Given its widespread usage, we asked how H9-derived hCO development and composition are affected by Matrigel dosage and delivery method. We found Matrigel exposure influences organoid size, morphology, and cell type composition. We also showed that greater amounts of Matrigel promote an increase in choroid plexus (ChP) cells, and this increase is regulated by the BMP4 pathway. These results illuminate the effects of Matrigel on H9-derived human cerebral organoid development and the importance of delivery mode and amount on organoid phenotype and composition.

2. Materials and Methods

2.1. hESC Cell Lines

H9 (WA09; WiCell, Madison, WI, USA) were grown in E8 media (STEMCELL Technologies, Vancouver, BC, Canada) in 6-well culture dishes (Greiner Bio-One, Kremsmünster, Austria) coated with 0.5 µg/mL Vitronectin (STEMCELL Technologies). Cells were passaged every 3–5 days as necessary using 0.5 mM EDTA (Invitrogen, Waltham, MA, USA).

2.2. Solubilized Matrigel

Matrigel (Corning, Corning, NY, USA) was allowed to thaw on ice for 1–2 h until liquid, while 50 mL falcon tube aliquots of cerebral organoid differentiation media were allowed to warm to room temperature. Matrigel was then added directly to the room-temperature media and pipetted up and down thoroughly (~20 times) to mix.

2.3. Cerebral Organoid Generation

hCOs were generated through modifying the Lancaster whole brain organoid protocol [1,2]. Stem cells were grown to 75% confluency before dissociation into a single cell suspension using EDTA and Accutase (Invitrogen). 9000 cells were plated into a low-attachment U-bottomed 96-well plate (Corning) in hESC media supplemented with 50 µM Y-27632 (LC Labs, Woburn, MA, USA) and 4 ng/mL β-FGF (Gibco, Waltham, MA, USA). hESC media contained DMEM-F12 (Gibco), 20% *v/v* knockout serum replacement (Gibco), 3% *v/v* fetal bovine serum (Corning), 1% *v/v* MEM-NEAA (Gibco), 1% *v/v* Glutamax (Gibco), and 7 µL/L β-mercaptoethanol (Amresco, Solon, OH, USA). After 48 h, half of the media was replaced with hESC media containing Y-27632 and β-FGF. After another 48 h, half the media was removed again and replaced with hESC media without Y-27632 and β-FGF. On day 6, each organoid was transferred to its own well of a 24-well ultra-low-attachment plate (Corning) with 500 µL of neural induction media containing DMEM-F12, 1% *v/v* N2 supplement (Gibco), 1% *v/v* MEM-NEAA, and 1% *v/v* Glutamax, and 50 µg/mL heparin (Sigma, St. Louis, MO, USA). On days 8 and 10, an additional 500 µL of media was added to each well. At day 11, media were removed and replaced with cerebral organoid differentiation media without vitamin A consisting of 50:50 DMEM-F12: Neurobasal (Gibco) mixture, 0.5% *v/v* N2 supplement, 1% *v/v* Glutamax, 0.5% *v/v* MEM-NEAA, 1% B27 supplement w/o vitamin A (Gibco), 1% *v/v* Penicillin/Streptomycin (Lonza, Walkersville, MD, USA), 3.5 µL/L β-mercaptoethanol, 12.5 µL/L 4 mg/mL Insulin (Gibco), and solubilized Matrigel (Corning). The plates were immediately placed on an orbital shaker at 105 RPM to prevent organoids from settling into the Matrigel on the plate surface. Media were replaced with fresh cerebral organoid differentiation media without vitamin A after 48 h. After an additional 48 h, media were replaced with cerebral organoid differentiation media with vitamin A, which contained same components except the B27 supplement w/o vitamin A is replaced with B27 supplement with vitamin A (Gibco). Media were replaced with fresh cerebral organoid differentiation media with vitamin A every 2–3 days as necessary. Matrigel was added to fresh media until the targeted number of applications for a condition had been achieved.

2.4. Cryosectioning and Immunohistochemistry

Tissues were fixed in 4% paraformaldehyde (Sigma) for 15 min at 4 °C followed by three 10 min PBS washes (Gibco). Tissues were placed in 30% sucrose overnight at 4 °C and then embedded in 10% gelatin/7.5% sucrose (Sigma) in PBS. Embedded tissues were flash-frozen in an isopentane (Sigma) bath between –50 and –30 °C and stored at –80 °C. Frozen blocks were cryosectioned (Epremedia, Kalamazoo, MI, USA) to 30 µm. For immunohistochemistry, sections were blocked and permeabilized in 0.3% Triton X-100 (Sigma) and 5% normal donkey serum (VWR) in PBS. Sections were incubated overnight with primary antibodies: rabbit anti-TUJ1 (1:100, Sigma T2200), goat anti-SOX2 (1:20, R&D Systems AF2018), mouse anti-Phospho-Vimentin (1:200, MBL International D076-3S), rabbit anti-EMX1 (1:50, Atlas Antibodies HPA006421), mouse anti-SATB2 (1:100, Abcam ab51502), mouse anti-Calretinin (1:100, Sigma MAB1568), rabbit anti-FOXG1 (1:1000, Abcam ab18259), sheep anti-TTR (1:100, Bio-Rad, AHP1837), mouse anti-TTR (1:100, R&D Systems, MAB7505), and rabbit anti-AQP1 (1:200, Abcam ab15080) in 0.3% Triton X-100, 5% normal donkey serum in PBS at 4 °C. Sections were then incubated with Alexa Fluor 488 and 647 conjugated secondary antibodies (1:250) in 0.3% Triton X-100 and 5% normal donkey serum in PBS for 2 h at RT, and nuclei were stained with 300 nM DAPI (Invitrogen). Slides were mounted using ProLong Antifade Diamond (Thermo Fisher, Waltham, MA, USA).

Images were taken using a Nikon AR confocal laser scanning microscope (Nikon, Tokyo, Japan). All samples within quantification experiments were imaged using the same laser intensity settings using the 10X, 20X, and 40X objectives. Quantifications were performed manually in FIJI. Organoid condition names were first removed, and the images randomized before quantification to avoid bias. A 10,000 by 10,000 grid was overlaid over the image and each grid was manually counted as positive for containing tissue if the grid contained DAPI+ cells. These grids were then remeasured, and regions were considered positive if TTR+ staining was present in the grid. At least 4 organoids per condition were collected and measured.

For cell density measurements, a region of interest was generated around the organoid DAPI outline. The area was then calculated. Cell density was measured through the calculation of the area fraction of DAPI+ to the total organoid area. At least 3 organoids per condition were collected and measured. For rosette measurements, a region of interest was generated around the organoid SOX2+ rosette outline. The area was then calculated. The average size of all rosettes from an organoid was calculated. At least 2 organoids per condition were collected and measured. For cell death measurements, a region of interest was generated around the organoid DAPI outline. The area of both DAPI and Caspase-3 within the organoid were then calculated. Finally, the cell death was calculated from the area fraction of Caspase/DAPI. At least 3 organoids per condition were collected and measured.

2.5. Granular Surface Phenotype Quantification

Images for size experiments were taken using an epifluorescence microscope with a documentation camera (Nikon). Quantifications were performed manually in FIJI. Organoids exhibiting more than 5 changes in curvature (2nd derivative) per 1 mm of the organoid edge were considered granular.

2.6. Inhibitor Treatment Experiments

hCOs were treated with either a physiologically relevant 2 µM dose of FAK Inhibitor 14 [23,24] (Tocris Biosciences, Bristol, UK), 100 ng/mL DKK-1 [25,26] (Peprotech, Cranbury, NJ, USA), 200 ng/mL of Noggin [27,28] (Peprotech), or an ultrapure water control (Invitrogen). Organoids were continually exposed to compounds as long as Matrigel remained in the media.

Images for size experiments were taken using an iPhone 11 Pro (Apple, Cupertino, CA, USA). All samples within quantification experiments were imaged using the same lighting and 1X zoom. Quantifications were performed manually in FIJI.

2.7. Statistical Analysis

All statistical comparisons were performed using one-way ANOVA with Tukey–Kramer post hoc analysis. The results were considered statistically significant if p -values < 0.05.

3. Results

Lancaster and colleagues developed a protocol for generating “whole brain” hCOs [15,22]. In this protocol, early organoids (<11 days) are embedded within Matrigel. In contrast, Velasco and colleagues added Matrigel in solubilized form when generating cortical hCOs. As Matrigel embedding is one of the most labor- and time-intensive steps of the whole brain hCO protocol, we asked if Matrigel could be added directly to the media in solubilized form and what concentration ranges would be appropriate. We generated hCOs following the Lancaster protocol [15,22] until Matrigel embedding (Figure 1A). Instead of embedding the hCOs in 30 μ L of Matrigel per the protocol, we added Matrigel directly to the cerebral organoid differentiation media at concentrations ranging from 0 to 3% v/v and lengths of time (in number of applications or media changes) ranging from 2 to 39 days beginning on day 11. Media were changed every 2–3 days. Due to differences in both concentrations and lengths of time, the total volumes of Matrigel added are also reported. Organoid size was significantly affected by the Matrigel amount added (Figure 1B,C). hCOs exposed to higher amounts of Matrigel in solution were larger compared to those embedded in Matrigel and to those not exposed to any Matrigel (Figure 1B,C).

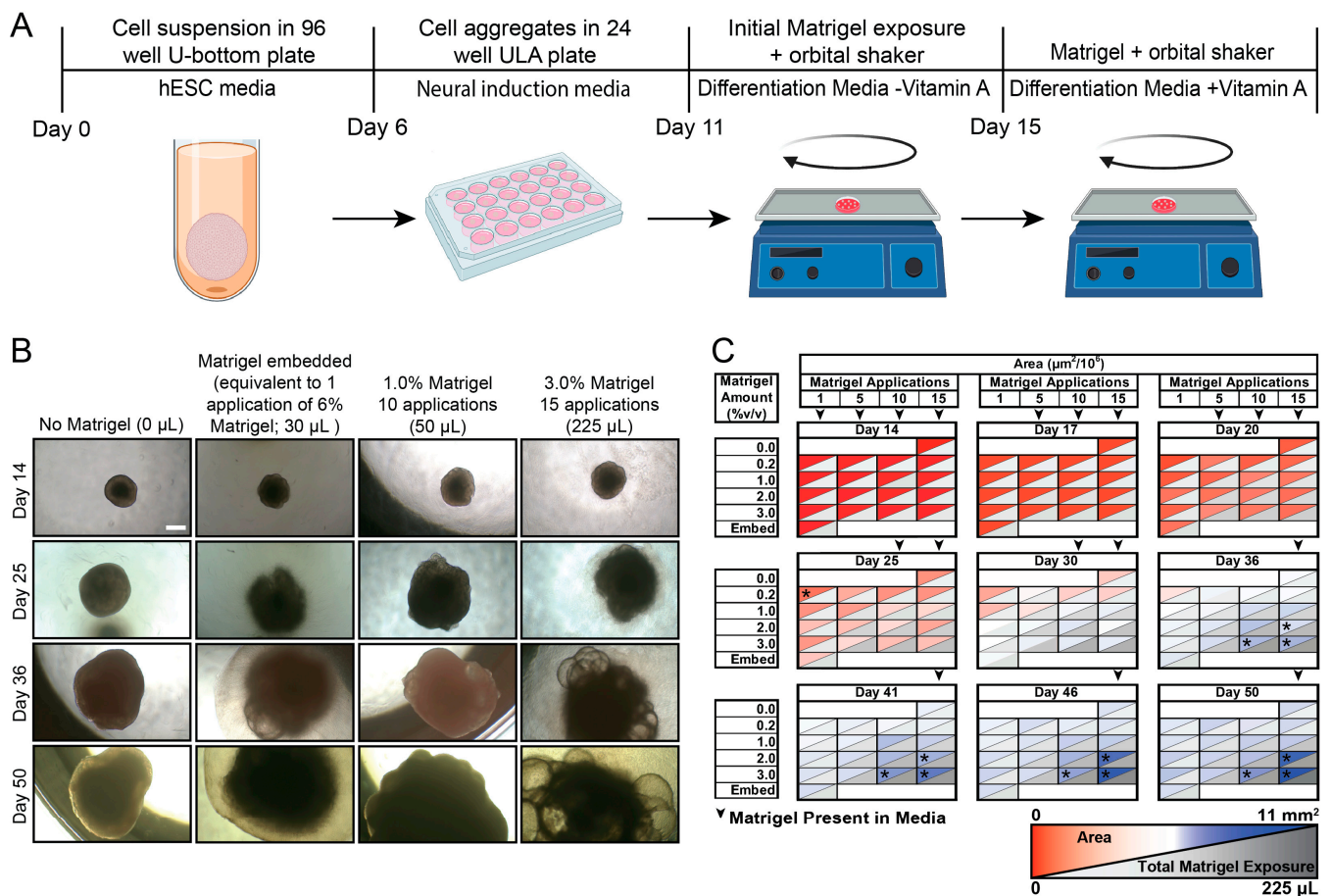


Figure 1. Amount of Matrigel in solution increases organoid size. (A) Schematic of experimental protocol, adapted from Lancaster and colleagues [15,22]. (B) Brightfield images of organoids with multiple Matrigel delivery regimens over a 50-day time course. Total Matrigel exposure shown in parentheses. Scale bar = 500 μ m. (C) Summary of hCO size measurements through time course experiment (mm^2). * p < 0.05, via one-way ANOVA relative to embedded (30 μ L) with Tukey–Kramer post hoc analysis, $n \geq 8$ organoids per condition.

From a simplistic perspective, the presence of growth factors in Matrigel might simply explain the monotonic relationship between size and Matrigel amount. However, in addition to hCO size, the amount of Matrigel affected gross hCO architecture. Three unique morphological hCO phenotypes correlated with low (<15 μ L total), medium (15–50 μ L total), and high (\geq 75 μ L total) amounts of Matrigel (Figure 2). Medium amounts of Matrigel yielded standard hCO phenotypes, characterized by a smooth, rounded surface and solid tissue [15,22] (Figure 2A). These hCOs contained diverse cell types which are characteristic of whole brain hCOs (Figure 2B). hCOs exposed to low amounts of Matrigel exhibited a thin, granular surface characteristic of non-neural epithelia [19] (Figure 2C). Interestingly, about 10% of hCOs that initially had a smooth surface developed a granular surface after removal of Matrigel relatively late in development (after 6 weeks; day 41) (Figure 2D). hCOs exposed to high levels of Matrigel developed large, fluid-filled cysts with a thin enveloping membrane (Figure 2E). Unlike the fluid-filled cysts of expanded neuroepithelium that sometimes develop in the standard protocol after initial exposure to Matrigel and hCO differentiation media between days 11 and 20 [15,22], these large fluid-filled cysts did not develop into thick, light-impermeable tissue. In addition to morphological analysis, additional hCO characteristics were assessed (Figure 2F). Interestingly, Matrigel absence resulted in larger rosettes which are characteristic of early organoid development [15,22], while cell death increased in only low-Matrigel conditions (<15 μ L).

We hypothesized the cystic phenotype would reflect distinct cellular composition. Due to similarities in the morphology of the large fluid-filled hCOs to the choroid plexus (ChP) hCOs generated by Pellegrini and colleagues [2], we hypothesized that high Matrigel exposure increased ChP differentiation. To test this, we immunostained for transthyretin (TTR), a transporter protein produced in the ChP (Figures 3A and S1). Compared to the embedded control, hCOs exposed to high-Matrigel conditions exhibited significantly increased numbers of TTR⁺ regions. Additionally, we examined whether the fluid-filled cysts of the ChP hCOs exhibited expected apical polarization [2]. We confirmed the correct apical–basal polarity of the ChP hCOs fluid-filled cysts through observing the co-localization of TTR with apical water transporter aquaporin-1 (AQP1) (Figures 3B and S1). Fluid-filled cysts exhibited co-localization of TTR with apical water transporter aquaporin-1 (AQP1), confirming correct apical–basal polarity (Figure 3B).

To develop a better understanding of how Matrigel might be driving ChP formation, we asked if the pharmacological inhibition of different signal transduction pathways might abrogate this process. Pellegrini and colleagues [2] induced ChP hCOs through pulsing with BMP4, a dorsal telencephalic morphogen, and CHIR, a WNT pathway activator. Interestingly, TGF- β is one of the growth factors present in Matrigel and shares overlapping signaling transduction pathways with BMP signaling [29], so we added an inhibitor of BMP4 signaling, Noggin. Additionally, we asked if the mechanical effects of Matrigel embedding might influence ChP formation. To this end, we used FAK inhibitor 14 [30] to negatively perturb mechanotransduction. Finally, we also used DKK1 to inhibit the WNT pathway. hCOs were generated and cultured in hCO differentiation media with 3% Matrigel in solution, and the inhibitors were added during the initial Matrigel exposure on day 11. While inhibitors did not strongly alter hCO size, the presence of Noggin significantly ablated the appearance of fluid-filled cysts to the level observed in control, Matrigel-embedded hCOs (Figure 4A). We further confirmed this effect through immunostaining for the ChP markers TTR and AQP1 (Figure 4B).

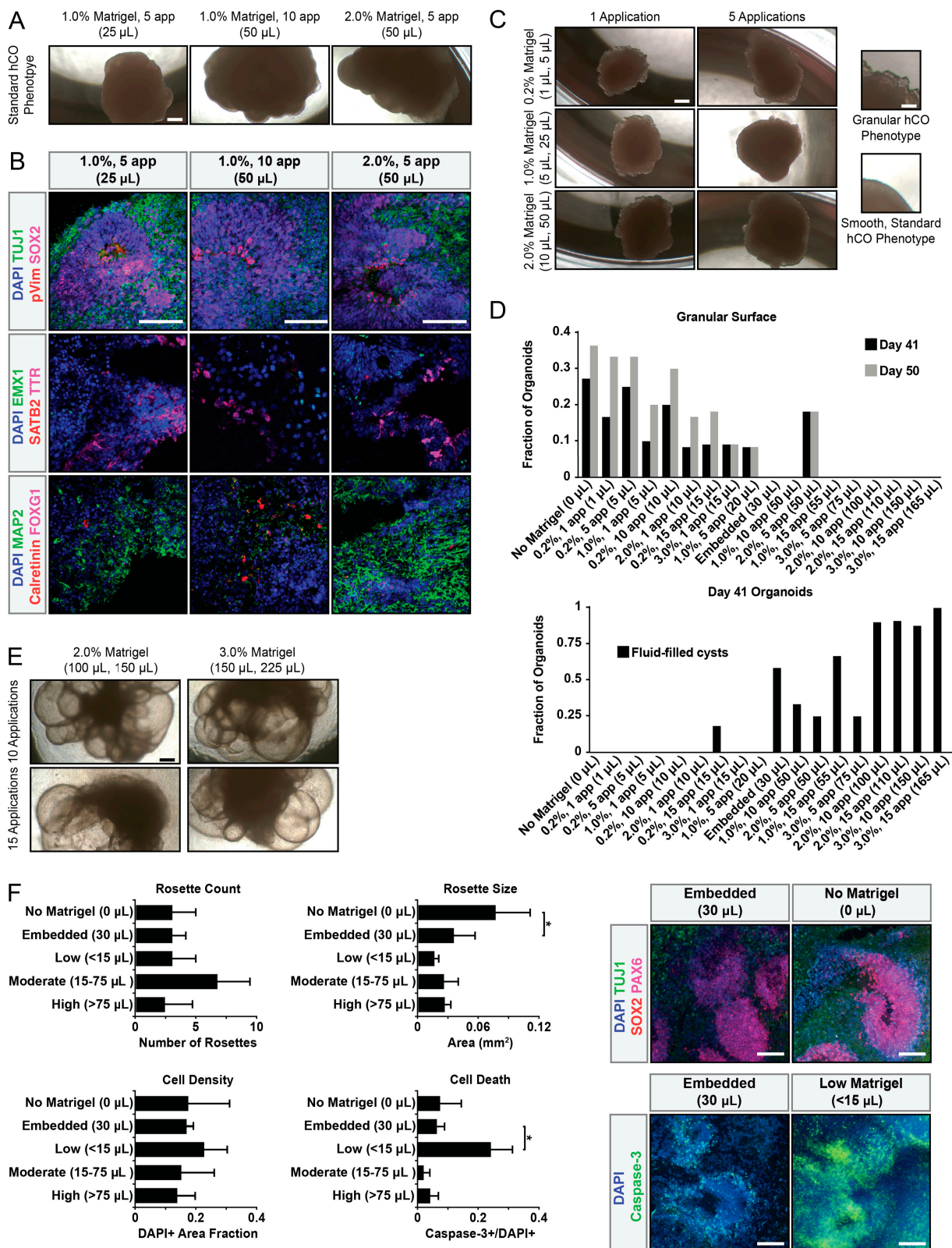


Figure 2. Soluble Matrigel dosage drives three distinct morphological phenotypes. **(A)** Brightfield images of standard hCO phenotype achieved with moderate Matrigel exposure (15–75 μ L). Total Matrigel exposure shown in parentheses. Scale bar = 500 μ m. **(B)** Moderate Matrigel exposure (15–75 μ L) drives standard hCO phenotype exhibiting broad cell type composition. Scale bars = 100 μ m. Total Matrigel exposure shown in parentheses. **(C)** Low Matrigel exposure (<15 μ L) creates hCOs with granular surfaces. Total Matrigel exposure shown in parentheses. Scale bars: left = 500 μ m; right (insets) = 50 μ m.

(D) Granular surface phenotype increases after Matrigel removal from media. (E) High Matrigel conditions (>75 μL) yield large fluid-filled cysts. Total Matrigel exposure shown in parentheses (top, bottom). Scale bar = 500 μm . (F) Developmental characteristics including rosette development, cell density, and cell death across different conditions. Total Matrigel exposure shown in parentheses. Organoids were generated in a single experiment in separate wells. * $p < 0.05$, via one-way ANOVA with Tukey–Kramer post hoc analysis, $n \geq 2$ organoids per condition. Error bars are 95% confidence intervals. Scale bars = 100 μm .

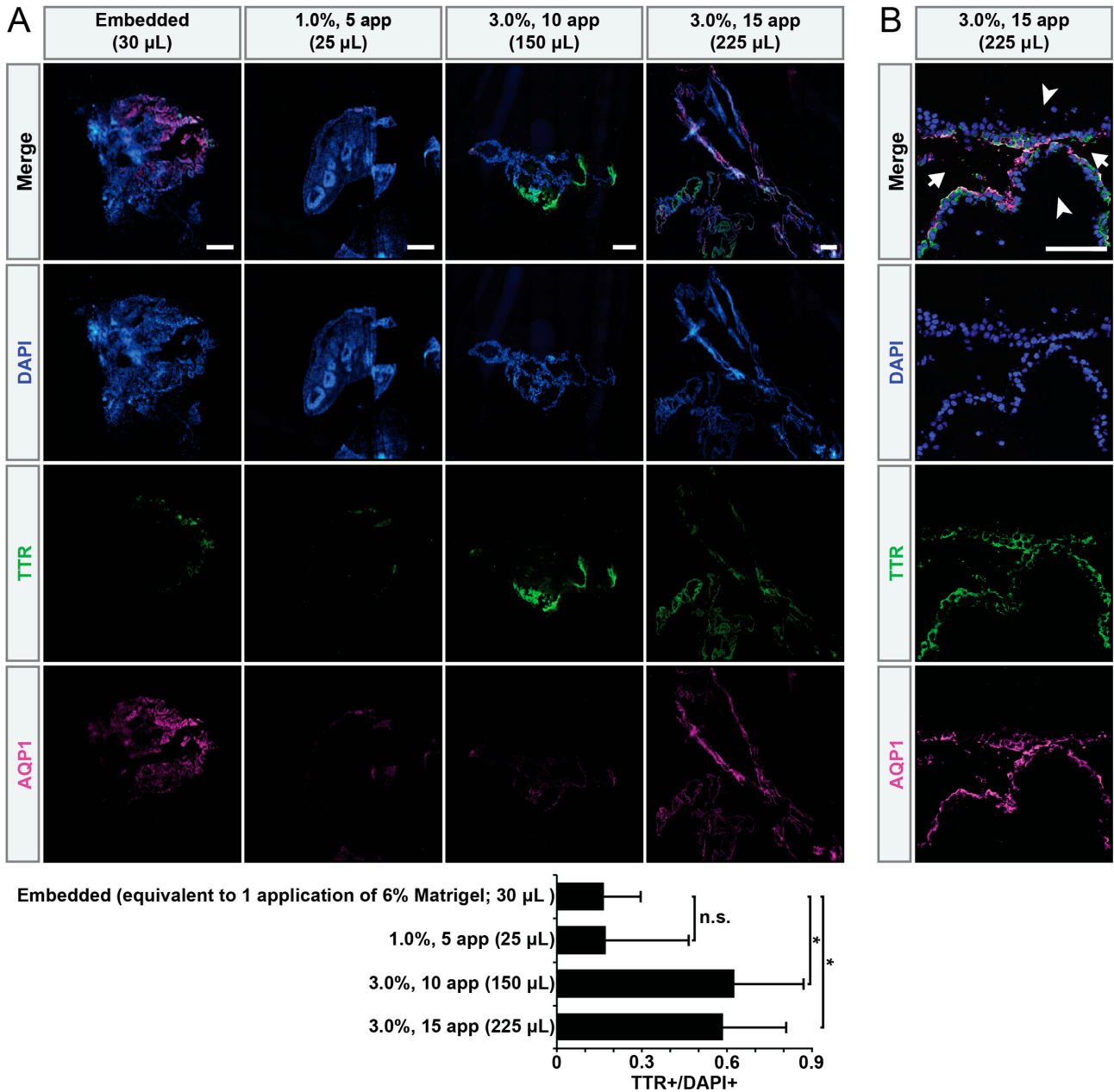


Figure 3. High-concentration Matrigel conditions promote ChP fate. (A) Immunostaining confirms hCOs with large fluid-filled cysts exhibit increased number of regions containing ChP cells. Total Matrigel exposure shown in parentheses. Organoids were generated in a single experiment in separate wells. * $p < 0.05$, n.s.: not significant, via one-way ANOVA with Tukey–Kramer post hoc analysis, $n \geq 4$ organoids per condition. Error bars are 95% confidence intervals. Scale bars = 500 μm . (B) Immunostaining reveals ChP cysts exhibit the expected polarization (apical side: arrows; basal side: arrow heads). Total Matrigel exposure shown in parentheses. Scale bar = 100 μm .

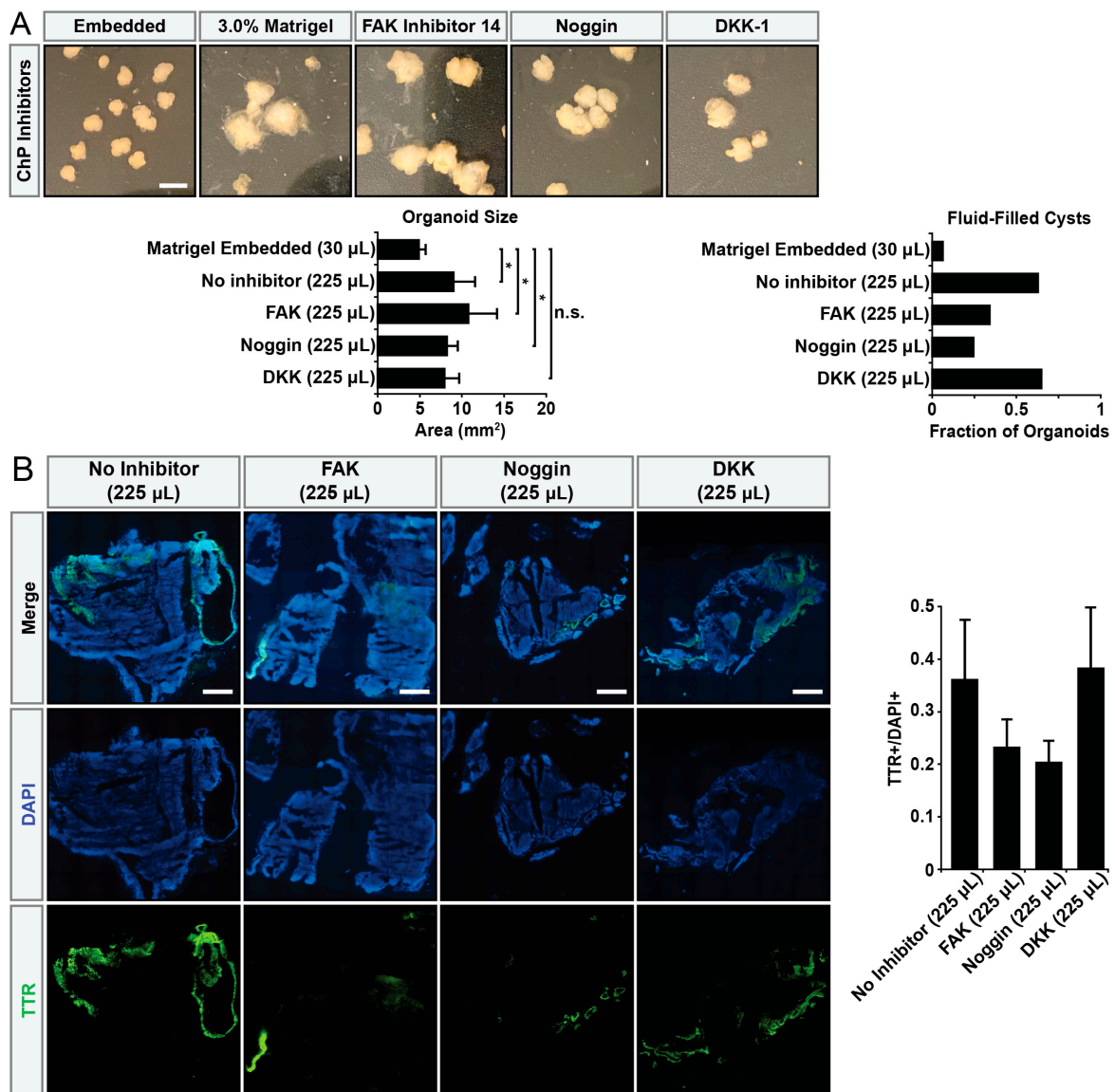


Figure 4. Matrigel promotes ChP differentiation through the BMP4 pathway. **(A)** Brightfield images showing gross morphological differences between hCOs generated in the presence of different pathway inhibitors. Total Matrigel exposure shown in parentheses. Organoids were generated in a single experiment in separate wells. * $p < 0.05$, n.s.: not significant, via one-way ANOVA with Tukey–Kramer post hoc analysis, $n \geq 18$ organoids per condition. Error bars are 95% confidence intervals. Scale bar = 500 μm . **(B)** Immunostaining confirms reduction in the number of ChP cells in the presence of Noggin. Total Matrigel exposure shown in parentheses. Error bars are 95% confidence intervals, $n \geq 3$ organoids per condition. Scale bars = 500 μm .

4. Discussion

We have shown that hCO growth and development is strongly influenced by Matrigel dosage and delivery method. A traditional hCO phenotype results from moderate levels of soluble Matrigel exposure, while high soluble Matrigel exposure promotes organoid ChP differentiation through the BMP4 pathway, consistent with literature [31,32]. This highlights the tunability of cerebral organoid cell type composition with Matrigel. Through carefully regulating the amount of Matrigel organoids are exposed to or the timing of the exposure, the composition of cerebral organoids can be tuned.

This work reinforces the need for caution when developing and executing protocols, including those beyond cerebral organoids. For example, many non-neural organoid pro-

protocols currently require Matrigel, such as those of the liver, heart, and kidney. Similar examinations in those systems may be warranted, even as the specific factors within Matrigel that affect development in different tissues will likely be different. In addition, there are many new competing matrices that have been developed, including Geltrex, LunaGel, ExtragelMatrix, and Cultrex, that will likely have varying compositions in addition to variabilities introduced between lots of these matrices. This work emphasizes the need to understand the dose-dependent effects of any matrix material used in organoid protocols.

Even when Matrigel is not used, this work illustrates the strong change in effect that can occur over relatively small changes in the concentration of a media component. This may explain the variability in organoid phenotypes and quality often observed and reported in the field. Substantial work has been pursued to attempt to replace reagents such as Matrigel [33–46], but it is a complex task to be able to replace all the complex components and functions of such matrices. Perhaps more broadly, the entire media composition for stem cell-derived systems including organoids could be revisited. This is because the media components driving these protocols remain largely derivative of prior base media historically used in cell culture, for example, DMEM media bases. It is unclear if these are still the most appropriate base media compositions for stem cell-derived systems, and if the same effects seen here with Matrigel would be altered or shifted when the base media are changed.

It is important to consider that while these studies shed light on the ability of Matrigel to tune H9-derived hCOs based on dosage, further work should be carried out to explore whether similar effects are observed in other cell lines. Variability between stem cell lines and their propensities to differentiate into different cell and tissue types is well known [47–50]. If upheld in other cell lines, using soluble Matrigel addition for whole brain hCO generation would significantly reduce the time and labor of organoid experiments through circumventing the most time-intensive step in the hCO generation process and enabling higher throughput and more comprehensive experiments to be carried out. It would also be interesting to explore if similar effects are observed when Matrigel is delivered in a solid form, with potential mechanobiological mechanisms also contributing in those cases to organoid development [51].

We also observed two more detailed but interesting phenotypes. In the absence of Matrigel, we observed larger rosettes, which are usually observed early in organoid development and yield larger numbers of rosettes further in development [15,22]. This may suggest that the absence of Matrigel stunts or pauses organoid development. In addition, we observed an increase in cell death only in low-Matrigel conditions (<15 μ L) but not in the absence of Matrigel. This may suggest low Matrigel is sufficient to induce additional organoid maturation or induce cell proliferation and differentiation but not sufficient to trophically fully support that development.

Finally, a significant impact of this work is providing a simple method for studying the ChP. Despite its essential functions in producing cerebrospinal fluid and acting as the blood–CSF barrier, the ChP has been understudied due to its relatively inaccessible location within the brain, the surrounding vasculature, and its structural fragility [52–54]. This work provides another valuable tool to address biological questions pertaining to the ChP. Overall, this analysis emphasizes the importance of careful attention to detail required when using, altering, or developing cerebral organoid protocols.

Supplementary Materials: The following supporting information can be downloaded at: <https://www.mdpi.com/article/10.3390/organoids2040013/s1>, Table S1: Supplemental Data. Figure S1: High Resolution Images Highlighting TTR+ Region Morphology. Scale bars = 100 μ m.

Author Contributions: Conceptualization, R.C.E. and A.J.K.; methodology, R.C.E. and A.J.K.; formal analysis, R.C.E. and A.J.K.; investigation, R.C.E. and J.E.O.; data curation, R.C.E. and A.J.K.; writing—original draft preparation, R.C.E. and A.J.K.; writing—review and editing, R.C.E. and A.J.K.; visualization, R.C.E. and A.J.K.; supervision, A.J.K.; project administration, A.J.K.; funding acquisition, A.J.K. All authors have read and agreed to the published version of the manuscript.

Funding: Research reported in this publication was supported by the National Institute On Drug Abuse of the National Institutes of Health under Award Number DP1DA044359. The content is solely the responsibility of the authors and does not necessarily represent the official views of the National Institutes of Health. The North Carolina State University Provost office provided additional support through the Professional Experience Program.

Institutional Review Board Statement: Not applicable.

Informed Consent Statement: Not applicable.

Data Availability Statement: Raw data are available in the Supplemental Materials.

Acknowledgments: We thank Zuzana Drobna, Dilara Sen, Balaji Rao, and Adam Mischler for their help and thoughtful insights.

Conflicts of Interest: The authors declare no conflict of interest.

References

1. Velasco, S.; Kedaigle, A.J.; Simmons, S.K.; Nash, A.; Rocha, M.; Quadrato, G.; Paulsen, B.; Nguyen, L.; Adiconis, X.; Regev, A.; et al. Individual brain organoids reproducibly form cell diversity of the human cerebral cortex. *Nature* **2019**, *570*, 523–527. [[CrossRef](#)] [[PubMed](#)]
2. Pellegrini, L.; Bonfio, C.; Chadwick, J.; Begum, F.; Skehel, M.; Lancaster, M.A. Human CNS barrier-forming organoids with cerebrospinal fluid production. *Science* **2020**, *369*, eaaz5626. [[CrossRef](#)] [[PubMed](#)]
3. Mariani, J.; Simonini, M.V.; Palejev, D.; Tomasini, L.; Coppola, G.; Szekely, A.M.; Horvath, T.L.; Vaccarino, F.M. Modeling human cortical development in vitro using induced pluripotent stem cells. *Proc. Natl. Acad. Sci. USA* **2012**, *109*, 12770–12775. [[CrossRef](#)] [[PubMed](#)]
4. Qian, X.; Nguyen, H.N.; Song, M.M.; Hadiono, C.; Ogden, S.C.; Hammack, C.; Yao, B.; Hamersky, G.R.; Jacob, F.; Zhong, C.; et al. Brain-Region-Specific Organoids Using Mini-bioreactors for Modeling ZIKV Exposure. *Cell* **2016**, *165*, 1238–1254. [[CrossRef](#)]
5. Valiulahi, P.; Vidyawan, V.; Puspita, L.; Oh, Y.; Juwono, V.B.; Sittipo, P.; Friedlander, G.; Yahalomi, D.; Sohn, J.-W.; Lee, Y.K.; et al. Generation of caudal-type serotonin neurons and hindbrain-fate organoids from hPSCs. *Stem Cell Rep.* **2021**, *16*, 1938–1952. [[CrossRef](#)]
6. Eura, N.; Matsui, T.K.; Luginbühl, J.; Matsubayashi, M.; Nanaura, H.; Shiota, T.; Kinugawa, K.; Iguchi, N.; Kiriya, T.; Zheng, C.; et al. Brainstem Organoids From Human Pluripotent Stem Cells. *Front. Neurosci.* **2020**, *14*, 538. [[CrossRef](#)]
7. Cederquist, G.Y.; Ascioia, J.J.; Tchieu, J.; Walsh, R.M.; Cornacchia, D.; Resh, M.D.; Studer, L. Specification of positional identity in forebrain organoids. *Nat. Biotechnol.* **2019**, *37*, 436–444. [[CrossRef](#)]
8. Delepine, C.; Pham, V.A.; Tsang, H.W.S.; Sur, M. GSK3 β inhibitor CHIR 99021 modulates cerebral organoid development through dose-dependent regulation of apoptosis, proliferation, differentiation and migration. *PLoS ONE* **2021**, *16*, e0251173. [[CrossRef](#)]
9. Amin, N.D.; Kelley, K.W.; Hao, J.; Miura, Y.; Narazaki, G.; Li, T.; McQueen, P.; Kulkarni, S.; Pavlov, S.; Paşca, S.P. Generating human neural diversity with a multiplexed morphogen screen in organoids. *bioRxiv* **2023**, 1–28. [[CrossRef](#)]
10. Sen, D.; Voulgaropoulos, A.; Keung, A.J. Effects of early geometric confinement on the transcriptomic profile of human cerebral organoids. *BMC Biotechnol.* **2021**, *21*, 59. [[CrossRef](#)]
11. Lancaster, M.A.; Corsini, N.S.; Wolfinger, S.; Gustafson, E.H.; Phillips, A.W.; Burkard, T.R.; Otani, T.; Livesey, F.J.; Knoblich, J.A. Guided self-organization and cortical plate formation in human brain organoids. *Nat. Biotechnol.* **2017**, *35*, 659–666. [[CrossRef](#)] [[PubMed](#)]
12. Kleinman, H.K.; Martin, G.R. Matrigel: Basement membrane matrix with biological activity. *Semin. Cancer Biol.* **2005**, *15*, 378–386. [[CrossRef](#)] [[PubMed](#)]
13. Kohen, N.T.; Little, L.E.; Healy, K.E. Characterization of Matrigel interfaces during defined human embryonic stem cell culture. *Biointerphases* **2009**, *4*, 69–79. [[CrossRef](#)] [[PubMed](#)]
14. Hughes, C.S.; Postovit, L.M.; Lajoie, G.A. Matrigel: A complex protein mixture required for optimal growth of cell culture. *Proteomics* **2010**, *10*, 1886–1890. [[CrossRef](#)]
15. Lancaster, M.A.; Renner, M.; Martin, C.-A.; Wenzel, D.; Bicknell, L.S.; Hurles, M.E.; Homfray, T.; Penninger, J.M.; Jackson, A.P.; Knoblich, J.A. Cerebral organoids model human brain development and microcephaly. *Nature* **2013**, *501*, 373–379. [[CrossRef](#)]
16. Yiangou, L.; Ross, A.D.; Goh, K.J.; Vallier, L. Human Pluripotent Stem Cell-Derived Endoderm for Modeling Development and Clinical Applications. *Cell Stem Cell* **2018**, *22*, 485–499. [[CrossRef](#)]
17. Fang, Y.; Eglén, R.M. Three-Dimensional Cell Cultures in Drug Discovery and Development. *SLAS Discov. Adv. Sci. Drug Discov.* **2017**, *22*, 456–472. [[CrossRef](#)]
18. Aisenbrey, E.A.; Murphy, W.L. Synthetic alternatives to Matrigel. *Nat. Rev. Mater.* **2020**, *5*, 539–551. [[CrossRef](#)]
19. Giandomenico, S.L.; Sutcliffe, M.; Lancaster, M.A. Generation and long-term culture of advanced cerebral organoids for studying later stages of neural development. *Nat. Protoc.* **2021**, *16*, 579–602. [[CrossRef](#)]
20. Bagley, J.A.; Reumann, D.; Bian, S.; Lévi-Strauss, J.; Knoblich, J.A. Fused cerebral organoids model interactions between brain regions. *Nat. Methods* **2017**, *14*, 743–751. [[CrossRef](#)]

21. Martins-Costa, C.; Pham, V.; Sidhaye, J.; Novatchkova, M.; Peer, A.; Möseneder, P.; Corsini, P.S.; Knoblich, P.A. Morphogenesis and development of human telencephalic organoids in the absence and presence of exogenous ECM. *bioRxiv* **2022**, 1–28. [[CrossRef](#)]
22. Lancaster, M.A.; Knoblich, J.A. Generation of cerebral organoids from human pluripotent stem cells. *Nat. Protoc.* **2014**, *9*, 2329–2340. [[CrossRef](#)]
23. Su, Y.; Besner, G.E. Heparin-binding EGF-like growth factor (HB-EGF) promotes cell migration and adhesion via focal adhesion kinase. *J. Surg. Res.* **2014**, *189*, 222–231. [[CrossRef](#)] [[PubMed](#)]
24. Hyvärinen, L.; Ojansivu, M.; Juntunen, M.; Kartasalo, K.; Miettinen, S.; Vanhatupa, S. Focal adhesion kinase and ROCK signaling are switch-like regulators of human adipose stem cell differentiation towards osteogenic and adipogenic lineages. *Stem Cells Int.* **2018**, *2018*, 2190657. [[CrossRef](#)] [[PubMed](#)]
25. Rudibaugh, T.P.; Tam, R.W.; Estridge, R.C.; Keung, A.J. Single cell assessment of human stem cell derived mesolimbic models and their responses to substances of abuse. *bioRxiv* **2023**. [[CrossRef](#)]
26. Wei, L.; Chen, C.; Ding, L.; Mo, M.; Zou, J.; Lu, Z.; Li, H.; Wu, H.; Dai, Y.; Xu, P.; et al. Wnt1 Promotes EAAT2 Expression and Mediates the Protective Effects of Astrocytes on Dopaminergic Cells in Parkinson's Disease. *Neural Plast.* **2019**, *2019*, 1247276. [[CrossRef](#)]
27. Manfrin, A.; Tabata, Y.; Paquet, E.R.; Vuaridel, A.R.; Rivest, F.R.; Naef, F.; Lutolf, M.P. Engineered signaling centers for the spatially controlled patterning of human pluripotent stem cells. *Nat. Methods* **2019**, *16*, 640–648. [[CrossRef](#)]
28. Yang, X.; Niu, N.; Liang, C.; Wu, M.-M.; Tang, L.-L.; Wang, Q.-S.; Lou, J.; Song, B.-L.; Zheng, W.-W.; Ma, H.-P.; et al. Stimulation of Epithelial Sodium Channels in Endothelial Cells by Bone Morphogenetic Protein-4 Contributes to Salt-Sensitive Hypertension in Rats. *Oxidative Med. Cell. Longev.* **2020**, *2020*, 3921897. [[CrossRef](#)]
29. La Rosa, I.; Camargo, L.S.; Pereira, M.M.; Fernandez-Martin, R.; Paz, D.A.; Salamone, D.F. Effects of bone morphogenetic protein 4 (BMP4) and its inhibitor, Noggin, on in vitro maturation and culture of bovine preimplantation embryos. *Reprod. Biol. Endocrinol.* **2011**, *9*, 18. [[CrossRef](#)]
30. Zhou, J.; Aponte-Santamaría, C.; Sturm, S.; Bullerjahn, J.T.; Bronowska, A.; Gräter, F. Mechanism of Focal Adhesion Kinase Mechanosensing. *PLoS Comput. Biol.* **2015**, *11*, e1004593. [[CrossRef](#)]
31. Hébert, J.M.; Mishina, Y.; McConnell, S.K. BMP Signaling is required locally to pattern the dorsal telencephalic midline. *Neuron* **2002**, *35*, 1029–1041. [[CrossRef](#)] [[PubMed](#)]
32. Watanabe, M.; Kang, Y.-J.; Davies, L.M.; Meghpara, S.; Lau, K.; Chung, C.-Y.; Kathiriyai, J.; Hadjantonakis, A.-K.; Monuki, E.S. BMP4 sufficiency to induce choroid plexus epithelial fate from embryonic stem cell-derived neuroepithelial progenitors. *J. Neurosci.* **2012**, *32*, 15934–15945. [[CrossRef](#)] [[PubMed](#)]
33. Kim, S.; Min, S.; Choi, Y.S.; Jo, S.-H.; Jung, J.H.; Han, K.; Kim, J.; An, S.; Ji, Y.W.; Kim, Y.-G.; et al. Tissue extracellular matrix hydrogels as alternatives to Matrigel for culturing gastrointestinal organoids. *Nat. Commun.* **2022**, *13*, 1692. [[CrossRef](#)] [[PubMed](#)]
34. Giobbe, G.G.; Crowley, C.; Luni, C.; Campinoti, S.; Khedr, M.; Kretzschmar, K.; De Santis, M.M.; Zambaiti, E.; Michielin, F.; Meran, L.; et al. Extracellular matrix hydrogel derived from decellularized tissues enables endodermal organoid culture. *Nat. Commun.* **2019**, *10*, 5658. [[CrossRef](#)]
35. Orlando, G.; Booth, C.; Wang, Z.; Totonelli, G.; Ross, C.L.; Moran, E.; Salvatori, M.; Maghsoudlou, P.; Turmaine, M.; Delario, G.; et al. Discarded human kidneys as a source of ECM scaffold for kidney regeneration technologies. *Biomaterials* **2013**, *34*, 5915–5925. [[CrossRef](#)]
36. Zachos, N.C.; Kovbasnjuk, O.; Foulke-Abel, J.; In, J.; Blutt, S.E.; de Jonge, H.R.; Estes, M.K.; Donowitz, M. Human enteroids/colonoids and intestinal organoids functionally recapitulate normal intestinal physiology and pathophysiology. *J. Biol. Chem.* **2016**, *291*, 3759–3766. [[CrossRef](#)]
37. Gilpin, S.E.; Guyette, J.P.; Gonzalez, G.; Ren, X.; Asara, J.M.; Mathisen, D.J.; Vacanti, J.P.; Ott, H.C. Perfusion decellularization of human and porcine lungs: Bringing the matrix to clinical scale. *J. Heart Lung Transplant.* **2014**, *33*, 298–308. [[CrossRef](#)]
38. Capeling, M.M.; Czerwinski, M.; Huang, S.; Tsai, Y.-H.; Wu, A.; Nagy, M.S.; Juliar, B.; Sundaram, N.; Song, Y.; Han, W.M.; et al. Nonadhesive Alginate Hydrogels Support Growth of Pluripotent Stem Cell-Derived Intestinal Organoids. *Stem Cell Rep.* **2019**, *12*, 381–394. [[CrossRef](#)]
39. Baptista, P.M.; Siddiqui, M.M.; Lozier, G.; Rodriguez, S.R.; Atala, A.; Soker, S. The use of whole organ decellularization for the generation of a vascularized liver organoid. *Hepatology* **2011**, *53*, 604–617. [[CrossRef](#)]
40. Saheli, M.; Sepantafar, M.; Pournasr, B.; Farzaneh, Z.; Vosough, M.; Piryaee, A.; Baharvand, H. Three-dimensional liver-derived extracellular matrix hydrogel promotes liver organoids function. *J. Cell. Biochem.* **2018**, *119*, 4320–4333. [[CrossRef](#)]
41. DiMarco, R.L.; Dewi, R.E.; Bernal, G.; Kuo, C.; Heilshorn, S.C. Protein-engineered scaffolds for in vitro 3D culture of primary adult intestinal organoids. *Biomater. Sci.* **2015**, *3*, 1376–1385. [[CrossRef](#)] [[PubMed](#)]
42. Wylie, R.G.; Ahsan, S.; Aizawa, Y.; Maxwell, K.L.; Morshead, C.M.; Shoichet, M.S. Spatially controlled simultaneous patterning of multiple growth factors in three-dimensional hydrogels. *Nat. Mater.* **2011**, *10*, 799–806. [[CrossRef](#)] [[PubMed](#)]
43. Candiello, J.; Grandhi, T.S.P.; Goh, S.K.; Vaidya, V.; Lemmon-Kishi, M.; Eliato, K.R.; Ros, R.; Kumta, P.N.; Rege, K.; Banerjee, I. 3D heterogeneous islet organoid generation from human embryonic stem cells using a novel engineered hydrogel platform. *Biomaterials* **2018**, *177*, 27–39. [[CrossRef](#)] [[PubMed](#)]
44. Ng, S.S.; Saeb-Parsy, K.; Blackford, S.J.; Segal, J.M.; Serra, M.P.; Horcas-Lopez, M.; No, D.Y.; Mastoridis, S.; Jassem, W.; Frank, C.W.; et al. Human iPS derived progenitors bioengineered into liver organoids using an inverted colloidal crystal poly (ethylene glycol) scaffold. *Biomaterials* **2018**, *182*, 299–311. [[CrossRef](#)] [[PubMed](#)]

45. Cruz-Acuña, R.; Quirós, M.; Farkas, E.A.; Dedhia, P.H.; Huang, S.; Siuda, D.; García-Hernández, V.; Miller, A.J.; Spence, J.R.; Nusrat, A.; et al. Synthetic hydrogels for human intestinal organoid generation and colonic wound repair. *Nat. Cell Biol.* **2017**, *19*, 1326–1335. [[CrossRef](#)]
46. Cruz-Acuña, R.; Quirós, M.; Huang, S.; Siuda, D.; Spence, J.R.; Nusrat, A.; García, A.J. PEG-4MAL hydrogels for human organoid generation, culture, and in vivo delivery. *Nat. Protoc.* **2018**, *13*, 2102–2119. [[CrossRef](#)]
47. Sun, C.; Zhang, J.; Zheng, D.; Wang, J.; Yang, H.; Zhang, X. Transcriptome variations among human embryonic stem cell lines are associated with their differentiation propensity. *PLoS ONE* **2018**, *13*, e0192625. [[CrossRef](#)]
48. Ortmann, D.; Brown, S.; Czechanski, A.; Aydin, S.; Muraro, D.; Huang, Y.; Tomaz, R.A.; Osnato, A.; Canu, G.; Wesley, B.T.; et al. Naive Pluripotent Stem Cells Exhibit Phenotypic Variability that Is Driven by Genetic Variation. *Cell Stem Cell* **2020**, *27*, 470–481.e6. [[CrossRef](#)]
49. Volpato, V.; Webber, C. Addressing variability in iPSC-derived models of human disease: Guidelines to promote reproducibility. *DMM Dis. Model. Mech.* **2020**, *13*, dmm042317. [[CrossRef](#)]
50. Yang, X.; Chen, D.; Sun, Q.; Wang, Y.; Xia, Y.; Yang, J.; Lin, C.; Dang, X.; Cen, Z.; Liang, D.; et al. A live-cell image-based machine learning strategy for reducing variability in PSC differentiation systems. *Cell Discov.* **2023**, *9*, 53. [[CrossRef](#)]
51. Cassel de Camps, C.; Aslani, S.; Stylianesis, N.; Nami, H.; Mohamed, N.-V.; Durcan, T.M.; Moraes, C. Hydrogel Mechanics Influence the Growth and Development of Embedded Brain Organoids. *ACS Appl. Bio Mater.* **2021**, *5*, 214–224. [[CrossRef](#)] [[PubMed](#)]
52. Redzic, Z.B.; Segal, M.B. The structure of the choroid plexus and the physiology of the choroid plexus epithelium. *Adv. Drug Deliv. Rev.* **2004**, *56*, 1695–1716. [[CrossRef](#)] [[PubMed](#)]
53. Lehtinen, M.K.; Bjornsson, C.S.; Dymecki, S.M.; Gilbertson, R.J.; Holtzman, D.M.; Monuki, E.S. The choroid plexus and cerebrospinal fluid: Emerging roles in development, disease, and therapy. *J. Neurosci.* **2013**, *33*, 17553–17559. [[CrossRef](#)] [[PubMed](#)]
54. Lun, M.P.; Monuki, E.S.; Lehtinen, M.K. Development and functions of the choroid plexus–cerebrospinal fluid system. *Nat. Rev. Neurosci.* **2015**, *16*, 445–457. [[CrossRef](#)]

Disclaimer/Publisher’s Note: The statements, opinions and data contained in all publications are solely those of the individual author(s) and contributor(s) and not of MDPI and/or the editor(s). MDPI and/or the editor(s) disclaim responsibility for any injury to people or property resulting from any ideas, methods, instructions or products referred to in the content.